

ANALYSIS OF ORBITAL PREDICTION ACCURACY IMPROVEMENTS USING HIGH FIDELITY PHYSICAL SOLAR RADIATION PRESSURE MODELS FOR TRACKING HIGH AREA-TO-MASS RATIO OBJECTS*

Tom Kelecy⁽¹⁾, Moriba Jah⁽²⁾

⁽¹⁾The Boeing Company, 5555 Tech Center Drive, Suite 400, Colorado Springs, CO 80919, USA
Email: thomas.m.kelecy@boeing.com

⁽²⁾Air Force Research Laboratory, 535 Lipoa Parkway, Suite 200, Kihei, HI 96753, USA

ABSTRACT

Inactive high area-to-mass ratio (A/m) resident space objects (RSOs) in the geosynchronous orbit (GEO) regime pose a hazard to active GEO RSOs. This attribute results in their increased sensitivity to non-conservative force effects manifested as perturbations of mean motion, inclination and eccentricity. This work examines the sensitivity of the trajectory prediction accuracies to various fidelities of complexity in the modeling of the SRP acceleration contributions to the overall dynamics. A physics-based solar radiation pressure model which includes the effects of refraction and absorption from the Earth's atmosphere during penumbral transitions is implemented. Additionally, variations in the area with respect to the sun are examined using representative orbits with associated eclipsing cycles. The trajectory prediction errors from combined modeling errors show significant growth consistent with loss of tracking. The errors are, in general, non normally distributed given their rejection of the null hypothesis to a standard normal distribution in various normality tests. This contributes to the prediction errors through errors in the orbit determination assumptions.

1. INTRODUCTION

High area-to-mass ratio (A/m) [inactive] resident space objects (RSOs) in the geosynchronous orbit (GEO) regime pose a hazard to active GEO RSOs. The combination of non-conservative forces (i.e. solar radiation pressure (SRP), thermal re-radiation, and Earth albedo), and solar and lunar gravitational perturbations causes perturbations in the orbits of these RSOs. The high A/m nature of these RSOs results in their increased sensitivity to non-conservative force effects manifested as perturbations of mean motion, inclination and eccentricity. Their subsequent drift with respect to the Earth, combined with their time varying orientation with respect to the sun and transitions into and out of Earth's shadow, results in

many of these RSOs becoming "lost" after initial acquisition as they transition through periods of days to weeks out of view of any specific observing site. This work examines the sensitivity of the trajectory prediction accuracies to various fidelities of complexity in the modeling of the SRP acceleration contributions to the overall dynamics.

Most trajectory prediction and reconstruction processes treat penumbral and/or umbra eclipses as simple geometric models (cylindrical or dual conic), and assume an RSO fixed cross-sectional area with respect to the sun. A physics-based solar radiation pressure model which includes the effects of refraction and absorption from the Earth's atmosphere during penumbral transitions is implemented. Additionally, variations in the area with respect to the sun are examined using representative orbits with associated eclipsing cycles. Assumptions about the reflective properties of the object contribute toward additional errors. The overall trajectory prediction errors are examined for each independent potential source of error, both separately and combined, for a given range of orbit parameters. The characteristics of these errors, including the magnitudes and statistical distribution, are presented.

The goal of this study is to define the SRP modeling requirements for orbit determination (OD) and prediction processing that will allow improvement in successful RSO reacquisition so as to reduce the number of lost RSOs. The next section describes the sources of error in more detail. The simulation and analysis scenarios and strategy are then described, followed by a detailed summary of the error analysis results. Finally, the implication of these results to tracking, acquisition and OD performance are presented. The resulting models are to be incorporated into the General Mission Analysis Tool (GMAT) [co-developed by NASA and AFRL] to expand its capabilities for supporting RSO tracking and research.

* Approved for public release; distribution unlimited.

2. SOLAR RADIATION ERROR MODELS

The analysis in this paper focuses on perturbations resulting from errors in parameters associated with the SRP acceleration. The analysis further focuses on debris objects in the geosynchronous orbit regime having A/m values in the range of 0.5-20 m²/kg. Hence, the gravitational perturbations are limited to the dominant zonal harmonic (J2) since A/m dynamic effects are driven solely by non-conservative forces. The greater sensitivity to SRP perturbations owing to the relatively high A/m values are of interest in assessing the orbital prediction sensitivity to mis-modelling of SRP related parameters. Though subsequent work will address the impact to the orbital determination (OD) in detail, the results presented here will be used to outline their relevance to OD performance.

The SRP perturbation errors were analyzed, both individually and in combination, where the radial, in-track and cross-track (RIC) position and velocity errors were computed between an assumed “reference” trajectory and “perturbed” trajectory integrated over the same span of time, geometry, etc. The errors were based on assumed reference-perturbation differences in the following:

The SRP acceleration model used for this work incorporates both reflective and absorptive effects of the radiation incident on the RSO. The model accommodates any number of specified flat surfaces according to the equations

$$\vec{a}_{SRP} = -\frac{F_P}{c} \sum_{i=1}^{NS} \{ \Phi \vec{R}_i (\hat{k}_i \cdot \hat{n}_i) + \vec{P}_i \} Am \quad (1)$$

where the specular and diffuse reflection terms for each surface are defined as

$$\vec{R}_i = (1-s_i) \hat{k}_i - \frac{2}{3} d_i \hat{n}_i + 2(\hat{k}_i \cdot \hat{n}_i) s_i \hat{n}_i \quad (2)$$

the emission term is defined as

$$\vec{P}_i = \frac{2}{3} a_i \sigma T^4 \hat{n}_i \quad (3)$$

and the remaining parameters are defined as

$c = \text{speed of light}$

$s_i = \text{specular reflectivity of surface } i$

$d_i = \text{diffuse reflectivity of surface } i$

$a_i = \text{absorption of surface } i$

$\sigma = \text{Stefan - Boltzmann const.}$

$T = \text{surface temperature in deg Kelvin}$

The incident solar flux parameter, Φ , is adjusted according to the distance of the space object from the sun, but has a nominal (average) value of 1367 Watts/m² at distance of 1 Astronomical Unit (AU). Details of this computation can be found in [4]. The “size” parameter for each surface is defined as the area to mass ratio $Am_i = A_i / m$ for surface area A_i and mass m . The two unit vectors are defined as

$\hat{k}_i = \text{inertial unit direction of light incident on the surface}$

$\hat{n}_i = \text{inertial unit surface normal of area } A_i$

and it is worth noting that

$(\hat{k}_i \cdot \hat{n}_i) = \cos \text{ of the angle between incident light and unit surface normal}$

is an attitude dependent parameter. The surface normal unit vectors are defined in a “body” reference frame, and must be transformed to the inertial reference frame. Finally, the parameter Fp (the shadow function), in the interval [0, 1], is critical in this analysis being that it is the function used to model passage into and out of earth eclipse. The simplest geometric models are that of a cylinder or a conic/fractional [4], while the more complex pseudo-physical and physical models [4, 5, 6] attempt to account for the effects of atmospheric refraction and absorption of the incident light rays.

An example of the error in the shadow models is shown in Fig. 1 where the discrepancy between the cylindrical and physical models is plotted as a function of time, along with their differences, for a penumbral entry. The shadow model errors approach 50% over the 4-5 minute transition period. When multiple entry and exit errors are considered in the SRP acceleration computation, these can result in significant positional errors when integrated over a 7-day time span as shown in Fig. 2. This representative GEO object has an A/m = 10 m²/kg, resulting in an in-track error growth approaching 2 km at the end of the 7-day integration.

The RIC position error sensitivity for all combinations of shadow models was examined, and is summarized in Tab. 1 below. In general, as might be expected the largest errors occur between the purely geometric models (cylindrical and fractional) and physical models. These numbers can vary depending on the geometry of the eclipse entry and exit. The statistics are examined in more detail in §4 of this paper.

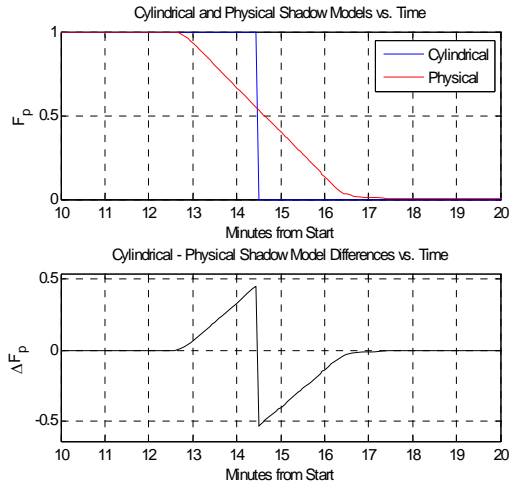


Figure 1. Cylindrical and Physical Shadow Model Penumbra Entry

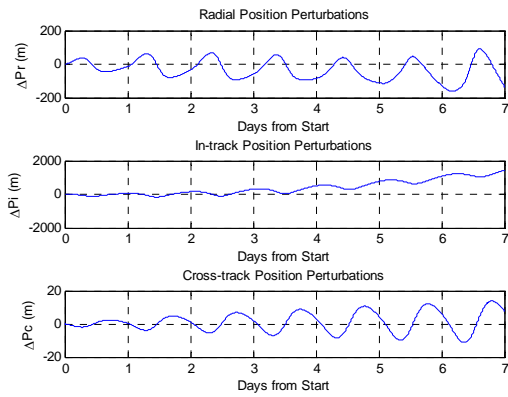


Figure 2. Cylindrical and Physical Shadow Model RIC Perturbations

Table 1. RIC Position Sensitivity to Shadow Models for 7-day GEO Propagation

Shadow Model Comparison	Radial (m)	In-track (m)	Cross-track (m)
Cylinder vs. Fractional	45	180	2
Cylinder vs. Pseudo-physical	200	2000	20
Cylinder vs. Physical	180	1800	80
Fractional vs. Pseudo-physical	200	2000	20
Fractional vs. Physical	200	1800	80
Pseudo-physical vs. Physical	50	500	5

3. SIMULATION ANALYSIS PROCESS

In order to analyze the complex interaction of the various sources of error, a Monte Carlo simulation was constructed in MATLAB to examine radial, in-track and cross-track (RIC) position and velocity errors for a range of orbit parameters, and for various combinations of shadow model, reflectivity and thermal emissions, attitude and A/m errors. The complex geometry of earth eclipse due to diverse orbits was considered by examining a range of representative orbits.

It must be noted that the Monte Carlo analysis draws samples from assumed *a priori* distributions using MATLAB's pseudo-random number generator. A more rigorous approach, making use of the Metropolis-Hastings algorithm and a true random number generator, will be implemented in future work. The analysis process is illustrated in Fig. 3, where each Monte Carlo run creates a randomly sampled reference orbit, and compares it to a "perturbed" orbit generated from randomly sampled initial conditions, namely orientation, reflection, thermal emission and A/m parameters. The reference and perturbed orbits were also compared where different shadow models were implemented in order to quantify and qualify the sensitivity of the trajectory errors to those error sources.

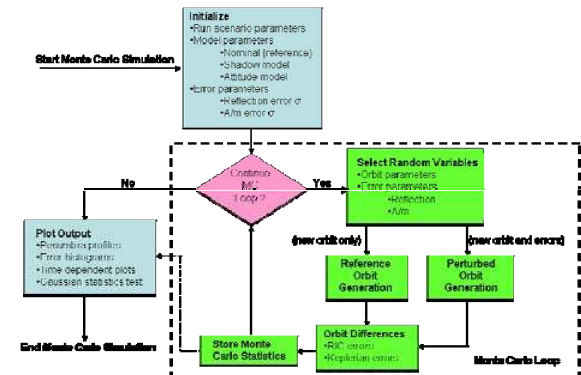


Figure 3. Monte Carlo Simulation Process

A Monte Carlo simulation was performed over a range of GEO orbit parameters, and for a set of RSO model parameter errors. For the orbit, the semi-major axis ranged from 38,000-46,000 km, the eccentricity over 0.0-0.4, and the inclination from 0-10 degrees. Errors in the diffuse and specular reflectivity values, and the absorption, were 30% each, while the A/m ratio error was based on a uniformly distributed 1% error.

The resultant trajectory errors were examined both separately (parametrically) and combined. The error sources that were examined were those due to the various shadow models, the reflectivity/absorption

coefficients, the knowledge of the A/m ratio, the RSO shape (number of surfaces) and assumed attitude (fixed vs. rotating). Nominal values for the RSO model parameters were $A/m = 10 \text{ m}^2/\text{kg}$, $s_i = 0.2$, $d_i = 0.8$ and $a_i = 0.2$.

The trajectory states were sampled from a uniform distribution for the ranges mentioned previously. The epoch was chosen from Day-of-year 90-100 (1-day span around the spring equinox), with the radial, in-track and cross-track (RIC) position and velocity errors examined for both 1-day propagation and 7-day propagation time spans. The mean, standard deviation and maximum deviation from “truth” for each of the RIC components (along with the total errors) were captured with the associated error distributions.

The integration interval was also to determine sensitivity to propagation through the eclipse boundaries. Errors were computed for runs that used a 30 second integration interval versus a 5 second integration interval. Those results indicate that care must be taken around the eclipse boundaries.

4. ERROR ANALYSIS RESULTS

A series of Monte Carlo simulations were conducted to examine the sensitivity to each of the sources of error, as well as their combined effect. Additionally, it is of interest to examine the distributions of the errors, and test them against the null hypothesis of normality since most orbit estimation processes assume that these errors are fully captured by the first and second moments of the distribution (i.e. a Gaussian assumption).

The total position mean and $1-\sigma$ errors are plotted in Fig. 4 below for each of the parametrically-examined error sources over the 7-day propagation period. The attitude errors are seen to be the dominant error source for this particular scenario, with material property errors (reflectivity and absorption) being the next dominant source. Though the 1% A/m errors are a distant third, these already reflect significant error as compared to the “truth”. The shadow model errors contribute the least error.

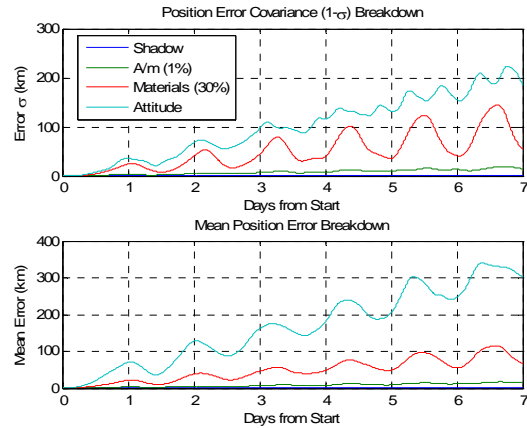


Figure 4. Position and Velocity Mean and $1-\sigma$ Errors for Component Error Sources

The total position and velocity mean and $1-\sigma$ errors are plotted in Fig. 5 below for the case where all error sources are combined over the 7-day propagation period. The mean error at a given time is plotted in black, while the $1-\sigma$ variations are plotted in red, and it can be seen that the position error approaches 500 km at the end of the 7-day period.

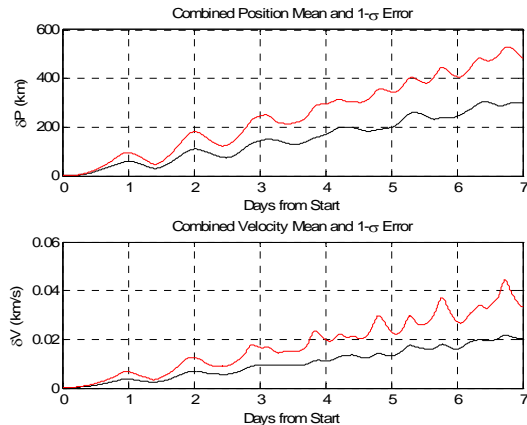


Figure 5. Position and Velocity Mean and $1-\sigma$ Errors for Combined Error Sources

The RIC position and velocity errors at the end of a 7-day propagation period were computed. These were tested for normality against the Shapiro-Wilk “W-test”, the Kolmogorov-Smirnov test, and the Lilliefors test [7]. It is worthy to note that the MATLAB pseudo-random number generator was tested for normality with all three tests, and the null hypothesis was accepted (i.e. the numbers generated were shown to belong to their assumed distributions). The error distributions for shadow model discrepancy (cylindrical vs. physical), a 1% error in A/m, a 30%

error in material properties (d_i , s_i and a_i), and attitude errors (fixed plate vs. rotating cube) were each examined as a 50 case Monte Carlo set.

Shadow Model Discrepancy (Cylindrical vs. Physical)

The total positional errors resulting from shadow model errors at the end of a 7-day propagation are shown in Fig. 6, where the maximum error is around 5 km, and the average between 1 km and 2 km. All three normality tests reject the null hypothesis of the data belonging to a standard normal distribution at the 5% level of confidence (i.e. there is 95% confidence in the data not belonging to a standard normal distribution).

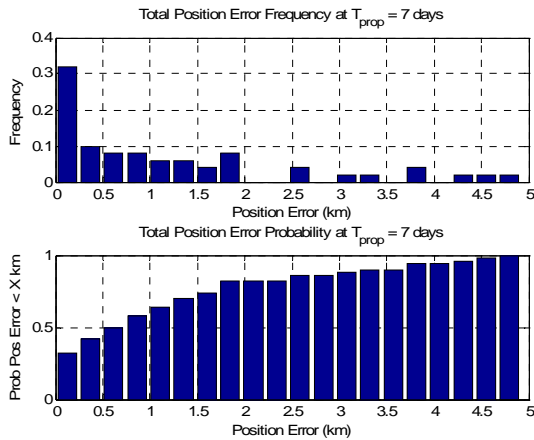


Figure 6. Total Position Error Distribution at 7-day Propagation Time – Shadow Model Errors
Total Error Gaussian Likelihood: 1% ($W = 0.807490$)

1% Error in A/m

The total positional errors resulting from 1% A/m model errors at the end of a 7-day propagation are shown in Fig. 7, where the maximum error is around 70 km, and the average between 10 km and 20 km. Again, all three normality tests reject the null hypothesis of the data belonging to a standard normal distribution at the 5% level of confidence.

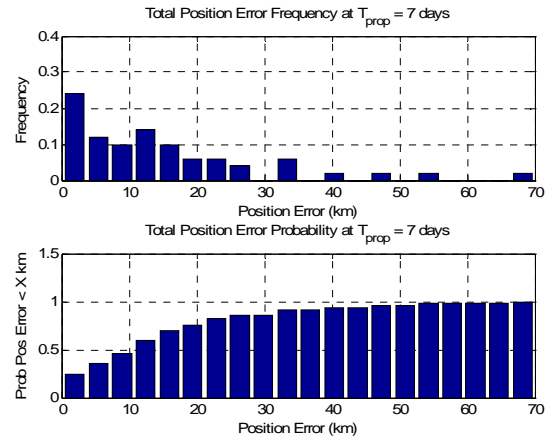


Figure 7. Total Position Error Distribution at 7-day Propagation Time – 1% A/m Errors
Total Error Gaussian Likelihood: 1% ($W = 0.829528$)

30% Error in Diffuse, Specular and Absorption Coefficients (d_i , s_i and a_i)

The total positional errors resulting from 30% reflection and absorption coefficient model errors at the end of a 7-day propagation are showing in Fig. 8, where the maximum error is around 250 km, and the average between 50 km and 100 km. All three normality tests were consistent with previous results.

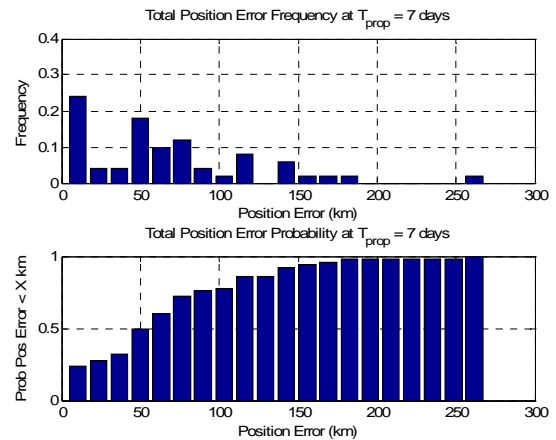


Figure 8. Total Position Error Distribution at 7-day Propagation Time – 30% s_i , d_i and a_i Errors
Total Error Gaussian Likelihood: 1% ($W = 0.893959$)

Attitude Errors (fixed plate vs. rotating cube)

The total positional errors resulting from attitude (fixed plate vs. rotation cube) model errors at the end of a 7-day propagation are showing in Fig. 9, where the maximum error is around 700 km, and the average

between 200 km and 300 km. All three normality tests were consistent with previous results.

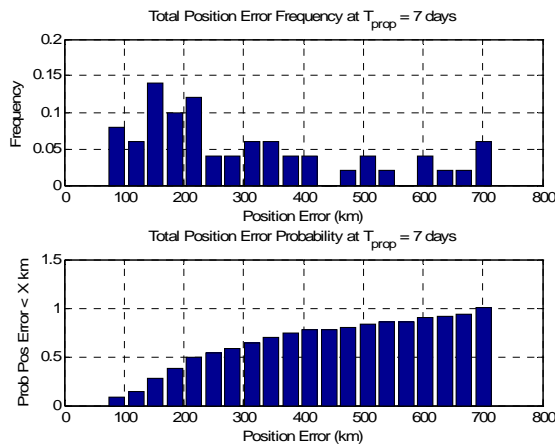


Figure 9. Total Position Error Distribution at 7-day Propagation Time – 50% Attitude Errors
Total Error Gaussian Likelihood: 1% ($W = 0.876397$)

All Errors Combined

The total positional errors resulting from all errors combined at the end of a 7-day propagation are showing in Fig. 7, where the maximum error is around 750 km, and the average between 200 km and 300 km. All three normality tests were consistent with previous results.

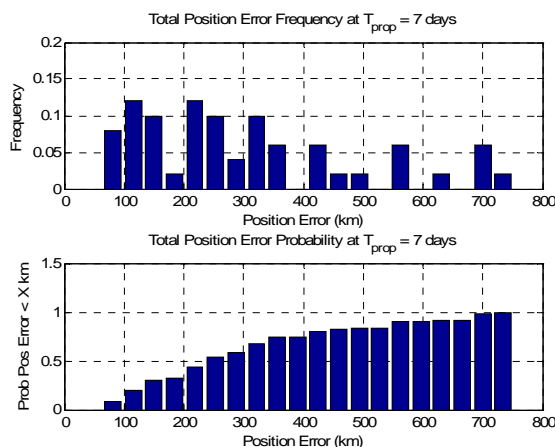


Figure 10. Total Position Error Distribution at 7-day Propagation Time
Total Error Gaussian Likelihood: 1% ($W = 0.903745$)

5. CONCLUSIONS

The Monte Carlo simulation results yield the RIC errors resulting from a 7-day propagation that includes shadow modeling errors, reflectivity and absorption coefficient errors, errors in the assumed A/m value, and errors in the assumed object orientation. The propagation errors appear to be most sensitive to the orientation assumptions, though all error sources contribute significantly to the prediction errors. Each source of error results in a non-Gaussian statistical distribution, both when examined independently and when combined. The resulting errors are large enough to result in loss of the object if re-acquisition is attempted after several days or more. Future work will examine the effect of implementing the Metropolis-Hastings algorithm for Monte Carlo sampling as a measure of appropriateness in the input random variables and statistics of the output. The resultant non-normality of the trajectory errors over time motivates the investigation of making use of estimation strategies such as Adaptive Gaussian Mixture filters [8], which approximate the true PDF by way of fitting multiple Gaussian distributions to what is inferred from the data. The “adaptive” aspect of this method is that in between observations, the relative weights assigned to each Gaussian component are propagated by constraining the weight estimates to minimize the predicted error in the Fokker-Planck-Kolmogorov equation. This equation is known to be the theory which describes the true evolution of any PDF.

6. REFERENCES

- Schildknecht, et al., “Properties of the High Area-to-mass Ratio Space Debris Population in GEO,” AMOS Tech. Conf., Wailea, Hawaii, Sept, 2005.
- Kececy, T., G. Stansbery, T. Payne and R. Thurston, “Solar Radiation Estimation and Analysis of a GEO Class of High Area-to-mass Ratio Debris Objects,” the American Astronautical Society (paper AAS 07-391) Astrodynamics Specialists Conference, Mackinac Island, MI, August 16, 2007.
- Kececy, T., E. Baker, P. Seitzer, T. Payne and R. Thurston, “Prediction and Tracking Analysis of a Class of High Area-to-mass Ratio Debris Objects in Geosynchronous Orbit,” ,” AMOS Tech. Conf., Wailea, Hawaii, Sept, 2008.
- Hujsak, R., “Solar Pressure,” Proceedings of the Artificial Satellite Theory Workshop, USNO, Nov. 8-9, 1993, pp 54-72.
- Vokrouhlicky, D., P. Farinella and F. Mignard, “Solar radiation pressure perturbations for Earth satellites: I. A complete theory including penumbra transitions,” Astron. Astrophys. 280, 295-312, 1993.

6. Vokrouhlicky, D., P. Farinella and F. Mignard, "Solar radiation pressure perturbations for Earth satellites: II. An approximate method to model penumbra transitions and their long-term orbital effects on LAGEOS," *Astron. Astrophys.* 285, 333-343, 1994.
7. Shapiro, S. and M. Wilk, "An Analysis of Variance Test for Normality (Complete Samples)," *Biometrika*, Vol. 52, No. 3/4, Dec., 1965, pp 591-611.
8. Terejanu, G., Singla, P., Singh, T., Scott, P., (2008) "Uncertainty Propagation for Nonlinear Dynamical Systems using Gaussian Mixture Models," *Journal of Guidance, Controls, and Dynamics* Vol.31, No.6, pp. 1623-1633